Journal of Inorganic Biochemistry 150 (2015) 81–89

Contents lists available at ScienceDirect

Journal of Inorganic Biochemistry

journal homepage: www.elsevier.com/locate/jinorgbio

The bacteriohemerythrin from *Methylococcus capsulatus* (Bath): Crystal structures reveal that Leu114 regulates a water tunnel

Kelvin H.-C. Chen [a,*,1], Phimonphan Chuankhayan [b,1], Hsin-Hui Wu [a,c], Chun-Jung Chen [b,d,e,**], Mitsuhiro Fukuda [f], Steve S.-F. Yu [g], Sunney I. Chan [g]

[a] *Department of Applied Chemistry, National Pingtung University, Pingtung 90003, Taiwan*
[b] *Life Science Group, Scientific Research Division, National Synchrotron Radiation Research Center, 30076 Hsinchu, Taiwan*
[c] *Institute of Bioinformatics and Structural Biology and Structural Biology Program, National Tsing Hua University, Hsinchu 30014, Taiwan*
[d] *Department of Biotechnology and Center for Bioscience and Biotechnology, National Cheng Kung University, Tainan 701, Taiwan*
[e] *Department of Physics, National Tsing Hua University, Hsinchu 30014, Taiwan*
[f] *Computer Chemistry Laboratory, Hyogo University of Teacher Education, 673-1494 Hyogo, Japan*
[g] *Institute of Chemistry, Academia Sinica, Taipei 11529, Taiwan*

ARTICLE INFO

Article history:
Received 30 January 2015
Received in revised form 1 April 2015
Accepted 1 April 2015
Available online 10 April 2015

Keywords:
Bacteriohemerythrin
Water tunnel
Methylococcus capsulatus (Bath)
Oxygen carrier protein
Autoxidation

ABSTRACT

The bacteriohemerythrin (McHr) from *Methylococcus capsulatus* (Bath) is an oxygen carrier that serves as a transporter to deliver O_2 from the cytosol of the bacterial cell body to the particulate methane monooxygenase residing in the intracytoplasmic membranes for methane oxidation. Here we report X-ray protein crystal structures of the recombinant wild type (WT) McHr and its L114A, L114Y and L114F mutants. The structure of the WT reveals a possible water tunnel in the McHr that might be linked to its faster autoxidation relative to hemerythrin in marine invertebrates. With Leu114 positioned at the end of this putative water tunnel, the hydrophobic side chain of this residue seems to play a prominent role in controlling the access of the water molecule required for autoxidation. This hypothesis is examined by comparing the autoxidation rates of the WT McHr with those of the L114A, L114Y and L114F mutants. The biochemical data are correlated with structural insights derived from the analysis of the putative water tunnels in the various McHr proteins provided by the X-ray structures.

1. Introduction

Classical hemerythrins (Hrs) are molecular oxygen carriers in certain marine invertebrates, such as sipunculids, brachiopods, priapulids, and annelids [1–4]. These proteins are found to exist in different oligomeric forms (α_n), including monomers (myohemerythrin (myoHr)), dimers, trimers, tetramers and octamers, each α monomer sharing a highly conserved four-helix bundle structure and a non-heme di-iron center as the O_2 binding site [5,6]. Hrs are not normally found in prokaryotes, though a Hr-like domain has been identified in the bacterial chemotaxis protein *Desulfovibrio vulgaris* chemoreceptor (DcrH-Hr) and has been structurally characterized [7–10]. Recently, Kao and coworkers have also reported a bacteriohemerythrin from *Methylococcus capsulatus* (Bath) (McHr), a monomeric form of hemerythrin co-expressed in this methanotroph when the bacterium is grown under high copper to biomass conditions to overproduce the particulate methane monooxygenase (pMMO) [11–13]. From the effects of the McHr on the activity of the pMMO, it has been proposed that McHr acts as a shuttle to transport dioxygen from the cytoplasm of the cell to the intracytoplasmic membranes for delivery of the O_2 to the pMMO enzyme for methane oxidation [14].

McHr has been cloned and over-expressed in *Escherichia coli* and the recombinant protein has been studied by various biophysical methods [13]. The protein has also been purified from *M. capsulatus* (Bath) cells for biophysical/biochemical characterization [11]. However, a crystal structure of the McHr has not been reported for comparison with the known structures of Hr from *Phascolopsis gouldii* [15], *Themiste dyscritum* [16], *Themiste pyroides* [17], and DcrH-Hr [7–9].

McHr delivers O_2 to the pMMO for the controlled oxidation of methane into methanol by the enzyme [11,12,14]. However, upon prolonged exposure to O_2 and water, oxy-McHr also undergoes autoxidation to form met-McHr and hydrogen peroxide [5,18], as with Hr from other species (Scheme 1). The rate of autoxidation varies from minutes to hours depending on the species of Hr. Mutagenesis studies of specific residues located in the vicinity of the di-iron center in Hr from the marine invertebrate *P. gouldii*, myohemerythrin (myoHr) and the bacterial DcrH-Hr have shed some structural insights into this issue [7–10, 15–17]. Kurtz and co-workers have discovered that the conserved Leu104 in myoHr (Leu98 in Hr, Leu115 in DcrH-Hr, and Leu114 in

* Correspondence to: K. Chen, No. 1 Lin-Sen Road, Pingtung City 90003, Taiwan. Tel.: +886 8 7226141x33254; fax: +886 8 7230305.
** Correspondence to: C.-J. Chen, No. 101 Hsin-Ann Road, Hsinchu 30076, Taiwan. Tel.: +886 3 5780281x7330; fax: +886 3 5783813.
E-mail addresses: kelvin@mail.nptu.edu.tw (K.H.-C. Chen), cjchen@nsrrc.org.tw (C.-J. Chen).
[1] Co-first author.

http://dx.doi.org/10.1016/j.jinorgbio.2015.04.001
0162-0134/

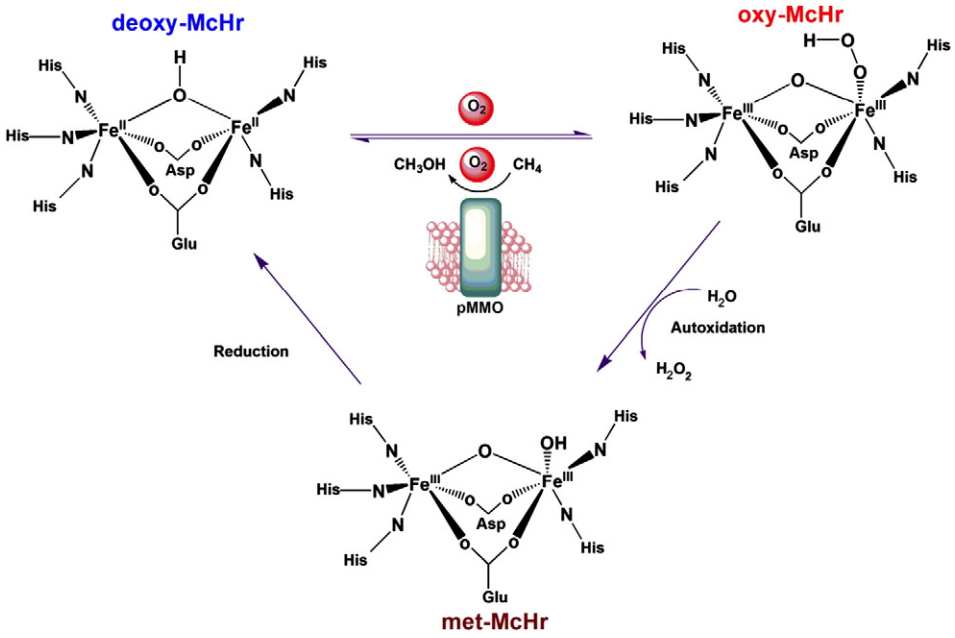

Scheme 1. The various states of hemerythrin from *M. capsulatus* (Bath). Shown are the oxidation states of the two iron atoms in the di-iron center together with the ligand environments in the deoxy-, oxy- and met-forms. The formation of oxy-McHr from doxy-McHr and the autoxidation of oxy-McHr to give met-McHr are also shown.

McHr) plays a critical role in limiting the entry of water molecules to reach the di-iron core [19]. Apparently, the hydrophobicity of the Leu104 residue controls the autoxidation and regulates the dioxygen binding properties of myoHr [15]. Subsequently, a water tunnel was identified in the crystal structure of DcrH-Hr, which was not found in Hr from marine invertebrates [7], and it was suggested that this water tunnel was the cause of the rapid autoxidation observed for DcrH-Hr. The autoxidation of McHr is also rapid, although not as fast as in the case of DcrH-Hr. Based on sequence alignment of McHr, DcrH-Hr, Hr and myoHr (Fig. 1) [20,21], Leu114 is part of a conserved WLVNHI alpha-helical motif forming the putative water tunnel. However, we surmise that the packing of this helix in the protein structure might affect the accessibility of solvent to the di-iron center [11].

In this study, we report ultra-high-resolution X-ray structures (~1.0 Å) on the recombinant wide-type (WT) McHr as well as on the L114A, L114Y and L114F McHr mutants. The WT McHr crystal structure demonstrates the existence of the putative water tunnel in McHr similar to DcrH-Hr, and we find that Leu114 indeed plays a prominent role at the end of the water tunnel controlling access of water to the di-iron core.

2. Experimental

2.1. Chemicals and reagents

All chemicals and reagents used in this study were of molecular biology grade or higher and were obtained from Sigma-Aldrich. Restriction enzymes were purchased from New England BioLabs.

2.2. Molecular cloning, site-directed mutagenesis and protein expression of the WT and recombinant McHr mutants

The cDNA encoding the McHr from *M. capsulatus* (Bath) was amplified by PCR and inserted into the tobacco etch virus (TEV) protease recognition site in the modified pGEX-4T-1 expression vector (GE Healthcare Inc.). The pET21a McHr WT was used as the template during the PCR experiments. The construct contained the glutathione S transferase (GST) fusion Tag. The L114A, L114F and L114Y mutants of McHr were constructed using the QuickChange® site-directed mutagenesis kit according to the manufacturer's protocol (Stratagene Inc.). The primers are shown in Supplementary Data Table A.1. The vector constructed was transformed into *E. coli* BL21 (DE3) cells (Novagen Inc.). A 5-liter vessel fermenter (Major Science Inc.) was used in the cell culture experiments. The bacteria were grown in Luria–Bertani (LB) medium in the presence of ampicillin (100 μg/mL) and chloramphenicol (34 μg/mL) at 37 °C until the cell density reached an OD_{600} of 0.6–0.8. The cultures were induced with 0.5 mM isopropyl β-D-thiogalactopyranoside (IPTG) for 3 h at 37 °C. The cells were harvested by centrifugation at 6000 rpm for 30 min at 4 °C followed by snap freezing in liquid nitrogen and stored at −80 °C.

2.3. Purification of the recombinant McHr proteins

Frozen bacterial pellets were re-suspended in the lysis buffer (50 mM Tris–HCl, 150 mM NaCl, pH 8.0), and the cells were lysed at 20,000 psi in a French Press. The cell lysate was then subjected to centrifugation at 27,000 ×*g* for 40 min followed by ultracentrifugation at 220,000 ×*g* for 1 h at 4 °C to remove the cell debris and the membrane fraction from the lysis solution. Subsequently, we collected the supernatant solution after further purification by passing the lysis solution through a 0.22-μm filter.

To obtain the purified recombinant McHr protein, the crude protein was incubated with glutathione agarose bead (Thermo Inc.) for 2 h in a 4 °C cold room. After washing the column with the lysis buffer, TEV protease was added into the column for 1 h at room temperature to remove the GST tag. The recombinant McHr protein was then eluted with elution buffer (50 mM Tris–HCl, 150 mM NaCl, pH 8.0). Finally, the eluted samples were concentrated and injected into a Superdex 75 column (GE Healthcare Inc.) with 50 mM Tris–HCl, 150 mM NaCl, pH 8.0, and the purified McHr was evaluated by using SDS-PAGE and UV–visible (UV–vis) spectroscopy.

2.4. Preparation of deoxy-, oxy- and met-forms of the recombinant McHr

The deoxy-form of the recombinant McHr was prepared by sodium dithionite treatment. The experimental procedures were carried out in an anaerobic glove box (type A vinyl anaerobic chamber, Coy Lab. Products Inc.) at room temperature. The purified recombinant McHr was dialyzed against ten equivalents of sodium dithionite to the protein

Fig. 1. Sequence alignment of hemerythrins and myohemerythrins. The alignments of the bacteriohemerythrins from *M. capsulatus* (Bath) (McHr) (NCBI:gi81682690), the hemerythrin-like domain in *D. vulgaris* (DcrH) (NCBI:gi6685084), *P. gouldii* hemerythrin (Phgou_hem) (NCBI:gi6694943) and *P. gouldii* myohemerythrin (Phgou_myo) (NCBI:gi253340) were performed by using Clustal X [20,21]. The four alpha helices forming the four-helix bundle secondary structure of McHr are given by α1, α2, α3, and α4 at the top of the first sequence, and the conserved Leu114 in McHr is highlighted in red and square frame. The amino acid residues supporting the assembly of the di-iron center are highlighted in bold and the WLVNHI motif is shown in italic.

concentration for 6 h and repeated twice to form the deoxy-McHr. Afterwards, the deoxy-McHr was dialyzed against degassed dithionite-free Tris–HCl buffer (pH 8.0) for 18 h in order to remove the excess sodium dithionite. To obtain the oxy- and met-forms of the McHr, the deoxy-McHr was directly exposed to air. UV–vis and X-ray absorption spectra confirmed the oxidation states of the various forms of the WT and mutated McHr.

2.5. Electrophoresis, metal analyses and amino acid sequencing of the recombinant McHr proteins

Electrophoresis was performed on a 13.3% acrylamide–SDS gel covered with a 4.5% acrylamide stacking gel. Both the 4.5% acrylamide stacking gel and the 13.3% acrylamide–SDS gel were prepared by using a stock solution containing 38.67% (wt/wt) acrylamide and 1.33% (wt/wt) N, N-bis-(methylene acrylamide). Electrophoresis was carried out at 100 V until the bromophenol blue marker reached the bottom of the gel (about 2.5 h). The gel was stained in a 0.25% (wt/vol) Coomassie brilliant blue G-250 solution containing 25% methanol for 20 to 30 min and then destained in a destaining solution containing 25% methanol and 7% acetic acid.

2.6. UV–vis absorption and X-ray absorption spectroscopy

UV–vis spectra were recorded at 1-nm resolution with a pair of quartz cells on a Hitachi U2900 UV–vis double beam spectrophotometer. X-ray absorption spectroscopy data were collected at the National Synchrotron Radiation Research Center, NSRRC (Beamline wiggler 17C, Si (111) double crystal monochromator) in Hsinchu. All samples were loaded into a sample holder (1.4 cm × 1.4 cm × 0.2 cm) covered with sheets of Kapton. During the measurements, the samples were maintained at room temperature. Fluorescence data were collected using a solid-state detector equipped with a Ni filter and Soller slits. The data represented an average of 9 scans. Data reduction included energy calibration assigning the first inflection point of Fe foil to 7112 eV.

2.7. Crystallization of the wild-type McHr and mutants

The WT McHr and mutants (L114A, L114Y and L114F McHr) were prepared in 50 mM Tris–HCl, 150 mM NaCl, pH 8.0 at a concentration of 34 mg/mL and screened with crystallization kits. The crystallization was performed with the hanging-drop vapor-diffusion method. Crystals of the WT McHr were first obtained from the crystallization screening kit with Memstar™ (molecular dimensions) containing polyethylene glycol (PEG) 400 (v/v, 2%) and ammonium acetate (2 M) in a sodium–HEPES buffer (100 mM, pH 7.5). The crystallization conditions for L114A, L114Y and L114F McHr were the same as for the WT McHr. Equal volumes (1 μL) of the protein solution and the corresponding crystallization reagent were mixed and equilibrated against the reservoir (100 μL). Crystals grew within one week at 18 °C. All the crystallizations were carried out in air without the addition of reductant. Thus, the crystals should correspond to those of the WT McHr and mutants in the met-form.

2.8. X-ray data collection

All crystals were cryo-protected with glycerol (20%) and frozen in liquid nitrogen before data collection. X-ray diffraction data were collected on beamlines 12B2 and 44XU at SPring-8 in Japan and on beamlines 13B1, 13C1 and 15A1 at NSRRC in Taiwan. All data were processed using *HKL2000* [22].

2.9. Crystal structure determination and refinement

The crystal structures of the WT McHr were determined by the molecular replacement method with *CCP4* [23] using the structure of DcrHHr as the search model (PDB code: 2AVK; amino-acid sequence identity 35%), and further model building was performed with *Coot* [24]. The structures of mutants L114A, L114Y and L114F McHr were determined by molecular replacement using the determined wild-type structure as the search model. All refinements were performed with the *refmac* program in *CCP4*. The correctness of the stereochemistry of the models was verified using *MolProbity* [25]. The rmsd (root mean square deviation) from ideality in ranges 0.007–0.010 Å for bond lengths and 1.400–1.626° for bond angles of all the structures calculated with *CCP4* shows a satisfactory stereochemistry. In the Ramachandran plot, all main-chain dihedral angles of the residues are in the most favored and additionally allowed regions. The structures have been deposited with PDB protein data bank (www.wwpdb.org) under the accession codes 4XPX, 4XPY, 4XQ1 and 4XPW. The figures were generated using *PyMol* (www.pymol.org). All crystallographic data and refinement statistics are summarized in Table 1.

Table 1
Statistics of X-ray data and structure refinement.

Protein	McHr-WT	L114A	L114Y	L114F
PDB ID	4XPX	4XQ1	4XPY	4XPW
Data collection				
Space group	*P*6	*P*6	*P*6	*P*6
Cell dimensions (Å)				
a, *b*, *c*	83.43, 83.43, 30.89	83.88, 83.88, 31.18	83.11, 83.11, 31.01	83.28, 83.28, 30.96
Resolution (Å)	24.08–1.03	27.45–1.40	23.49–1.13	24.84–1.17
R_{merge} (%)	5.8(43.8)	8.1(54.1)	5.5(22.4)	6.5(42.6)
Completeness (%)	99.7(99.8)	96.7(98.9)	97.2(99.6)	95.0(99.5)
Redundancy	4.5(13.2)	11.6(12.2)	4.4(10.4)	4.2(10.5)
Refinement				
Resolution (Å)	24.08–1.03	27.45–1.40	23.49–1.13	24.84–1.17
No. of reflections	57,799	22,962	43,683	39,403
R_{work}/R_{free} (%)	15.7/16.6	15.6/18.6	15.1/16.9	15.2/16.5
No. of atom				
Protein	1025	1030	1037	1036
Fe/O	2/2	2/1	2/2	2/2
Water	156	197	175	147
Average *B*-factor (Å^2)	13.0	14.3	12.4	12.4
rmsd				
Bond length (Å)	0.028	0.028	0.029	0.027
Bond angle (°)	2.204	2.293	2.226	2.286

Values in parentheses are for the highest-resolution shell.

3. Results

3.1. Preparation of the recombinant WT McHr and its variants

We have cloned and over-expressed the WT McHr and its L114A, L114Y and L114F mutants in *E. coli* as a fusion protein with the GST affinity tag in order to harvest sufficient quantities of the highly purified proteins for single-crystal X-ray diffraction and biochemical experiments. In each case, the recombinant McHr protein is isolated from the host *E. coli* cells following the standard procedures of French Press, ultracentrifugation and column chromatography. The cytoplasm of the cells is loaded onto a glutathione agarose open column pre-equilibrated with the lysis buffer. The bound protein is cleaved by TEV protease on the column and then eluted out by the lysis buffer. The highly purified recombinant McHr-containing fractions are collected by Äkta FPLC by size-exclusion chromatography using a superdex75 size-exclusion column. SDS-PAGE analysis shows that the recombinant WT, L114Y, L114F and L114A McHr proteins appeared as a highly purified polypeptide at 14.8 kDa (Fig. A.1).

3.2. UV–vis spectra

The UV–vis spectra of the purified WT McHr, L114F, and L114Y and L114A recombinants are summarized in Fig. 2a–c.

The UV–vis spectra of the purified deoxy-, oxy- and met-forms of the WT McHr (Fig. 2c) are identical to those previously reported for the hemerythrin purified from *M. capsulatus* (Bath). No UV–vis absorption features are discernible for the deoxy-form of the WT McHr. Upon exposure to the air, it is rapidly converted to the oxy-form with its characteristic μ-oxo to Fe(III) and -OOH to Fe(III) ligand-to-metal charge transfer bands at 328 nm and 371 nm, respectively. In the presence of air, the oxy-McHr is eventually converted to the met-form, as evidenced by slight shifts of the ligand-to-metal charge transfer (LMCT) bands to 327 nm and 376 nm, respectively. The autoxidation reaction half-time ($t_{1/2}$) is determined to be around 1 h, consistent with our previous report [11].

As with the WT McHr, no LMCT absorptions are observed for the purified deoxy forms of the L114F and L114Y McHr proteins. Upon exposure to air, both mutants are converted from the deoxy- to the oxy-forms just as fast as for the WT McHr. Again, the met-forms are obtained by continuous exposure of the oxy-McHr to air, but the autoxidation $t_{1/2}$ increases to 12 h and 20 h for the L114F and L114Y mutants, respectively. Fig. 2a and b shows the UV–vis spectra for the oxy-forms of these two mutants. In the case of the L114F McHr, LMCT bands are observed for the oxy-form at 320 nm and 371 nm, and for the met-form at 316 nm and 380 nm (Fig. 2a). The oxy- and met-L114Y McHr are purple in color, with a distinctive feature at 550 nm in the UV–vis spectrum due to the phenolate to Fe(III) charge transfer from the tyrosine residue, in addition to the charge transfer bands from the μ-oxo to Fe(III) in the region 337 to 330 nm (Fig. 2b).

Unexpectedly, only weak UV–vis absorptions are elicited for the as-isolated L114A McHr even after a 15-min purge with pure O_2 (Fig. 2c).

3.3. Metal analysis and near-edge X-ray absorption spectroscopy

Metal-ion analysis by atomic absorption spectroscopy shows that the recombinant WT and the three Leu114 McHr mutants contain 1.9–2.2 iron atoms per 14.8-kDa polypeptide. Near-edge X-ray absorption spectroscopy (Fig. 3) shows that the oxidation states of the iron atoms in the purified recombinant WT, L114F, L114Y and L114A McHr are mixed valence as isolated, similar to the ferrous ferric oxide (Fe_3O_4, Fe(II, III, III)), indicating that the WT and mutants McHr exist in the stable semi-met form in air as purified. It is interesting to note that, although one of the two irons apparently exists as Fe(III) in the L114A McHr as purified, no LMCT bands arising from μ-oxo- or oxo-charge-transfer to this Fe(III) are observed in the UV–vis spectrum. As described later, the crystal structure of this mutant reveals that a molecule of sodium nitrate is lodged near the non-heme di-iron site precluding dioxygen binding.

3.4. Crystal structures of the recombinant WT and mutant met-McHr: the water tunnel

Crystal structures of the DcrH-Hr protein have been previously reported by Chan et al. and Hayashi et al. [7,8]. Evidence for a putative water tunnel was provided in the structure of Chan et al. [7], and these workers suggested that rotation of the side chain of Leu115 at the end of the tunnel would open a channel to allow rapid access of a water molecule to the oxygenated non-heme di-iron center, facilitating the facile autoxidation ($t_{1/2} < 1$ min) required for detection of the dioxygen bound [7,19].

In this study, we have determined the protein structures for the WT met-McHr and its L114Y, L114F and L114A mutants at ultra-high

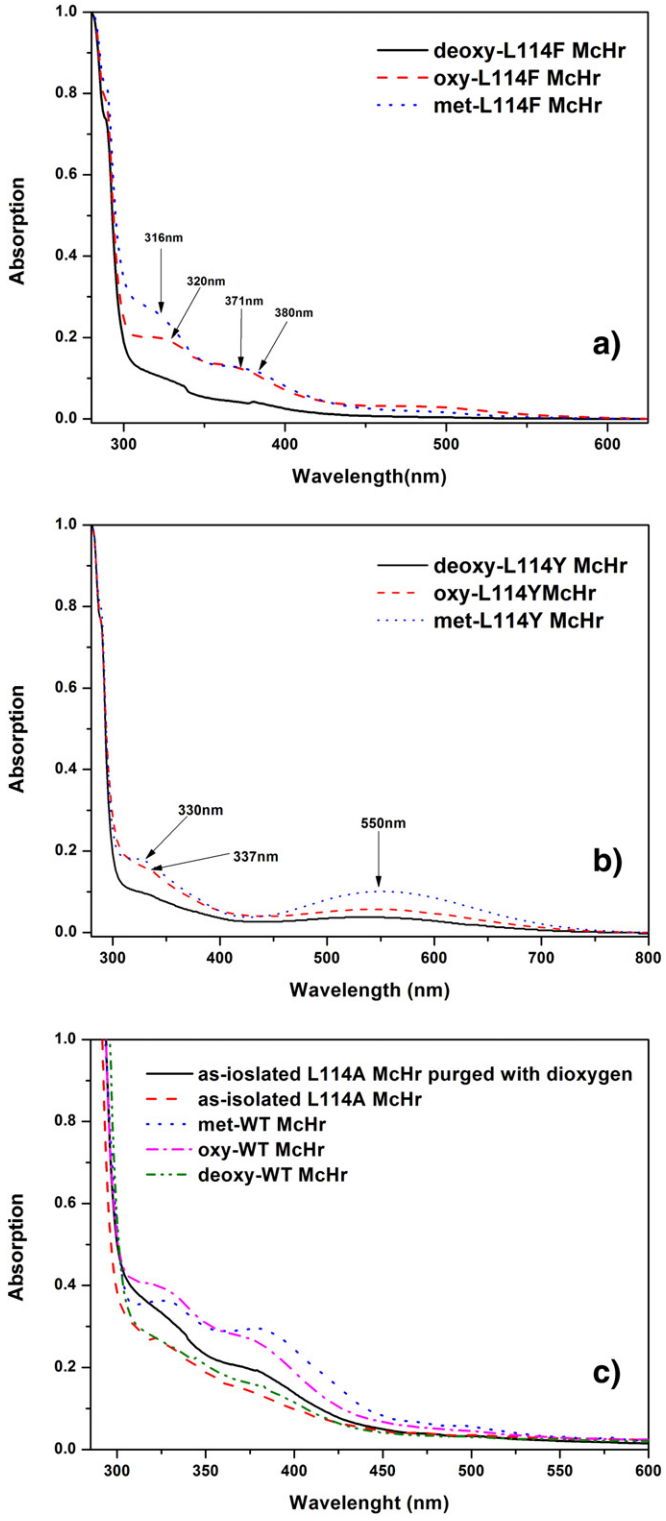

Fig. 2. (a) The UV–vis absorption spectra of the recombinant L114F McHr mutant in various iron oxidation states. The 300–400 nm absorption features are the characteristic μ-oxo to Fe(III) and -OOH to Fe(III) ligand-to-metal charge transfer bands. (b) The UV–vis absorption spectra of the recombinant L114Y McHr mutant in various iron oxidation states. The 300–400 nm absorption features arise from the characteristic μ-oxo to Fe(III) and -OOH to Fe(III) ligand-to-metal charge transfer bands associated with the oxygenated di-iron center. The 550 nm peak is assigned to the phenolate (114Y) to Fe(III) LMCT charge transfer absorption. (c) The isolated L114A McHr mutant exhibits no apparent UV–vis absorption. After a 15-min pure oxygen purge, a weak LMCT absorption is observed.

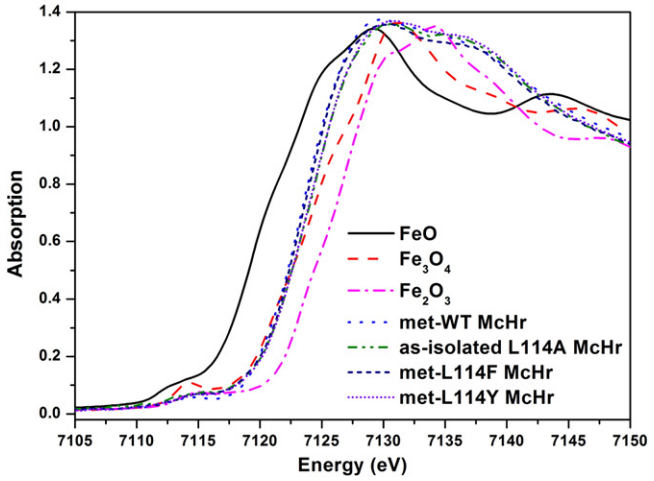

Fig. 3. The Fe K-edge X-ray absorption spectra of the purified recombinant met-WT, met-L114Y, met-L114F and as-isolated L114A McHr proteins together with various iron oxidation standards. Black line: FeO, Fe(II); red line: Fe_3O_4, Fe(II)(III)(III); blue line: Fe_2O_3, Fe(III)(III). Details of the X-ray absorption experiments are given in the text.

resolution (1.0–1.4 Å) with space group *P*6 (Table 1). Their overall structures are similar upon superimposition, with rmsd of ~0.11 Å for the Cα backbone between the structures of the WT met-McHr and the three mutants. These ultra-high resolution structures allow us to correlate

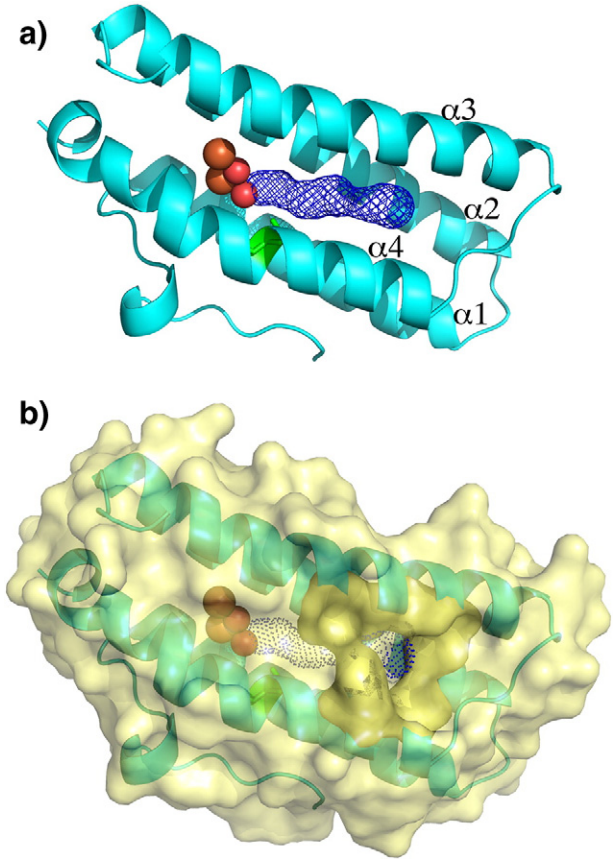

Fig. 4. (a) The protein crystal structure of the WT McHr comprises a four-helix bundle (light blue), a non-heme di-iron center (orange) and a water tunnel (deep blue mesh) oriented parallel with the long axis of the four-helix bundle. The oxygen molecule bound to the non-heme di-iron center and Leu114 is highlighted in red and green respectively. (b) Based on CAVER 3.0 transport pathway analysis, the putative water tunnel (deep blue dots) is shown to penetrate from the protein surface to the core of the di-iron center.

the autoxidation rates observed for the various McHr species with the water tunnel environments (Figs. 4 and 5). According to the protein X-ray crystallographic analysis, the WT met-McHr structure consists of a four-helix bundle (α1: 15–37, α2: 41–69, α3: 74–97 and α4: 103–129) with the non-heme di-iron center coordinated by His22, His58, His77, His81, His117, Asp122 and Glu62 (Fig. 5a).

Based on transport pathway analysis by CAVER 3.0 [26], we have located a putative water tunnel in the McHr oriented parallel to the long axis of the four-helix bundle. This water tunnel is lined by the side chains of the hydrophobic residues His22, Ile25, Val29, Leu32, Leu48, Leu51, Ile52, Val55, His58, Phe59, Glu62, His81, Leu84, Val87, Leu91, Phe109, Val110, Trp113, Leu114, His117, Ile118, and Asp122, and is terminated by the hydrophilic amino acids Cys88, Gln92, Thr106, and Thr107 adjacent to protein surface between helix α3 and α4 (Fig. 4a).

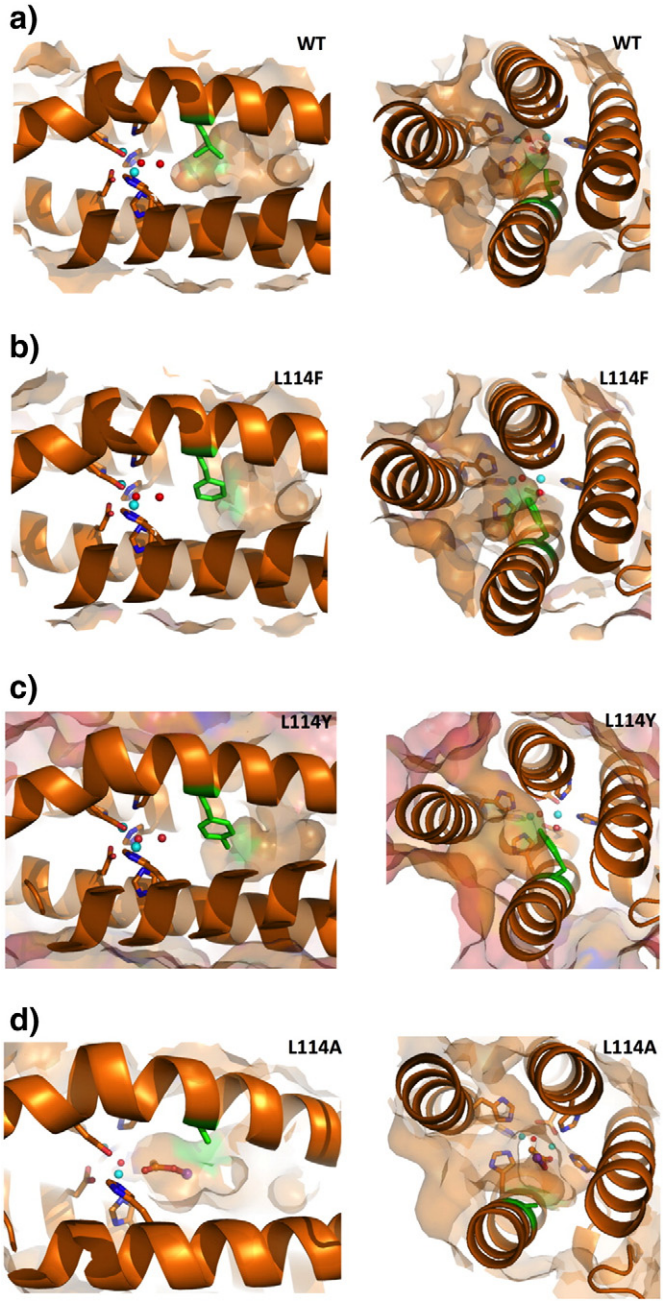

Fig. 5. The ultra-high-resolution X-ray structures of the recombinant WT met-McHr and three leucine 114 mutants: (a) WT; (b) L114F; (c) L114Y; and (d) L114A. Iron: sphere in blue; oxygen: sphere in red; amino acid mutated: stick in green; sodium acetate: stick in red and ball in purple.

According to our earlier study, the McHr autoxidation rate ($t_{1/2}$) is about 50 min, which is much faster than that observed for Hr from a marine invertebrate ($t_{1/2}$ = 20 h) [27–29]. In the L114F McHr mutant, the relatively larger phenyl side chain of phenylalanine (Phe) has replaced the branched aliphatic isobutyl side chain of the leucine (L114) in McHr. This substitution should result in steric effects in the opening and closing of the putative water tunnel (Fig. 5b). Consistent with this structural expectation, the autoxidation rate ($t_{1/2}$) measured for this mutant McHr is 20 h, which is similar to the marine invertebrates, and considerably slower than that in the WT McHr.

In the case of the recombinant L114Y McHr mutant, the side chain from tyrosine (Tyr) is expected to exhibit both steric and polar effects. The phenyl group here is similar in size to that in the L114F mutant, but the polar hydroxyl group of the tyrosine side chain will influence the affinity of water and its movement in the putative water tunnel (Fig. 5c). As expected, the $t_{1/2}$ of L114Y is 12 h, thus the autoxidation is relatively slower than in the case of the WT McHr, but significantly faster than for the L114F McHr mutant. Interestingly, the high-resolution X-ray protein structure of this L114Y mutant reveals that the mutated residue Tyr exhibits a double conformation in the vicinity of the active site, with the conformation of the side chain directed either toward the di-iron center or toward the putative water tunnel (Fig. 6).

In the L114A McHr mutant, the significantly smaller aliphatic methyl group has replaced the isobutyl side chain of Leu114 in McHr. Any steric effects associated with the opening and closing of the putative water channel should be diminished (Fig. 5d). Thus we would expect more facile solvent access to the di-iron site here. However, to our surprise, our biochemical experiments indicate that the as-isolated L114A mutant has lost the ability to form the oxy-McHr derivative. According to the crystal structure of the purified L114A McHr, a sodium acetate or sodium nitrate molecule is lodged near the non-heme di-iron site precluding dioxygen binding, and the putative water tunnel is completely open (Fig. 7). We cannot distinguish between an acetate anion from a nitrate. The F_o–F_c map can be fitted with either sodium acetate or sodium nitrate. The fitting results are shown in Supplementary Data Fig. A.2. Structure refinement gives a similar good density fitting with R_{work} and R_{free} values of 15.61 and 18.41% for NO_3^- and 15.49 and 18.28% for CH_3COO^- as the anion. We assume that the L114A McHr mutant has received the sodium acetate or sodium nitrate from the inorganic salts in the LB medium used to culture the host *E. coli* cells, or from the ammonium acetate/sodium nitrate in the HEPES buffer used in the crystallization of the protein.

3.5. Crystal structure of the WT met-McHr: comparison with the met-forms of DcrH-Hr and the invertebrate Hrs

The crystal structure of the WT met-McHr displays the same μ-oxo bridged di-iron metal center previously reported for the DcrH-Hr and met-Hrs from invertebrates. A close view of the non-heme di-iron site

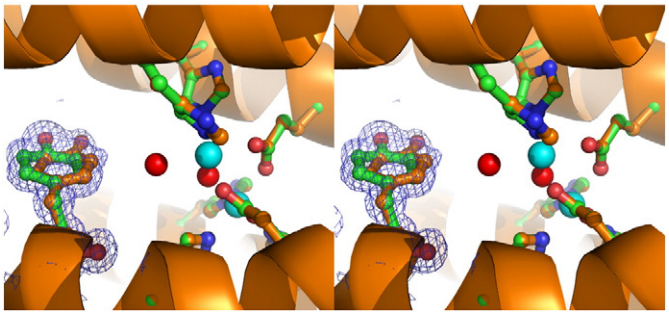

Fig. 6. The high-resolution X-ray protein structure of the met-McHr L114Y mutant reveals a double conformation of the mutated Tyr114 side chain with clear electron density (blue mesh) seen in the vicinity of the active site, with one conformation directed either toward the di-iron center (brown) and the other toward the putative water tunnel (green) shown in a stereo view.

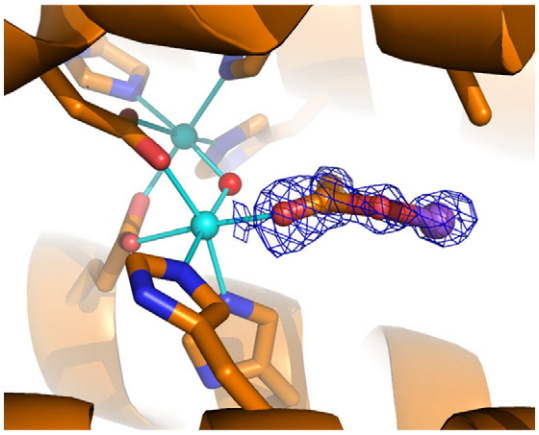

Fig. 7. A putative molecule of sodium acetate (blue mesh) is shown lodged near the non-heme di-iron site, precluding the binding of dioxygen to the di-iron center in the purified L114A met-McHr. The sodium cation is shown in purple. The omitted $2F_o - F_c$ electron density map is contoured at 2.3 σ.

is shown in Fig. 8, where we compare the geometries and bond distances of the two Fe atoms with the surrounding residues and O atoms between the different species of hemerythrins. The coordination environments and the iron–ligand bond distances of the μ-oxo bridged di-iron center in McHr are analogous to those found in previous met-Hr

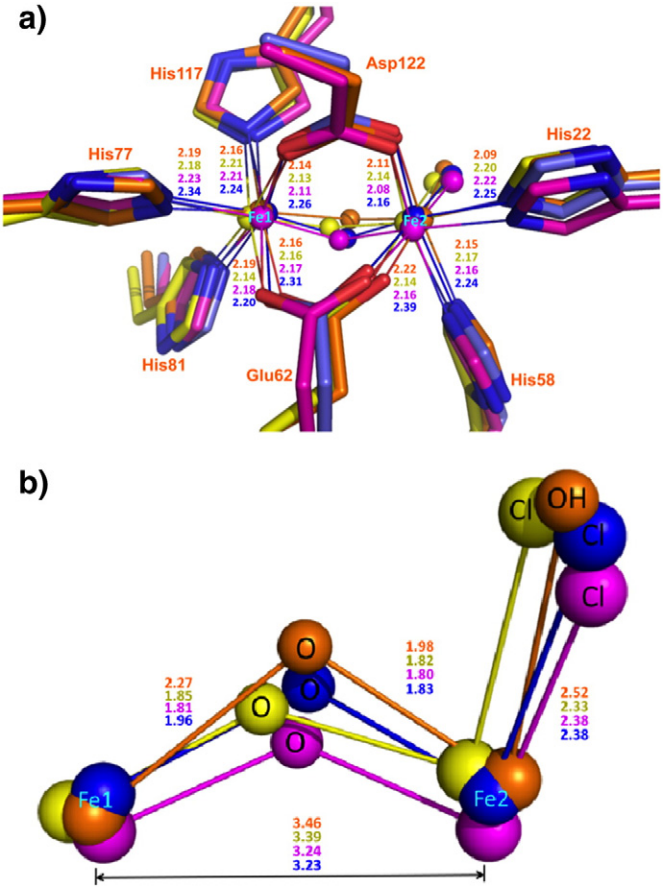

Fig. 8. Superimposed structures of the di-iron site in met-McHr (orange), met-DcrH-Hr from *D. vulgaris* (PDB: 2AWY; yellow), met-myoHr from *T. zostericola* (PDB: 1A7D; magenta) and met-Hr from *P. gouldii* (PDB: 1I4Y; blue). (a) The geometries and bond distances of the Fe atoms with their associated amino acid residues; and (b) zoom-in views of the Fe—O—Fe linkage at the non-heme di-iron site in the various met-Hrs.

structures (Fig. 8a). Fe1 is six-coordinated, with the ligands His77, His81, His117, Asp122 and Glu62. A hydroxide and the protein ligands His22, His58, Asp122 and Glu62 are associated with Fe2. The Fe1–Fe2 distance (3.46 Å) in WT met-McHr (Fig. 8b) is similar to that in DcrH-Hr (3.39 Å) [7] but it is significantly longer than those found in met-Hrs (3.23 Å and 3.24 Å) from invertebrates [15].

4. Discussion

It is conceivable that the different putative functions of various classes of hemerythrins are reflected in their autoxidation behaviors. A hemerythrin from a marine invertebrate is assumed to possess a dioxygen storage function, employing the non-heme di-iron center to bind O_2 within its vascular system for delivery to tissues when and where needed. Consistent with this function, the autoxidation of the oxy-Hr is extremely slow, with a half-life $t_{1/2}$ of ~20 h before it is autoxidized to the met-form [27–29]. In contrast, the autoxidation $t_{1/2}$ of oxy-DcrH-Hr, the hemerythrin-like domain in the fusion protein from *D. vulgaris*, is less than 1 min [10]. In the X-ray crystal structure of this DcrH-Hr, Chan and coworkers have previously identified a water tunnel that might facilitate the rapid autoxidation of the oxy-DcrH-Hr [7]. In addition, they have proposed that this rapid autoxidation is consistent with the function of this hemerythrin-like fusion domain as the dioxygen sensor in the chemotaxis receptor, which utilizes a redox-dependent conformational change to transduce a sensory signal to the neighboring methylation domain. The sensory mechanism could involve simple rotation of the side chain of Leu98 in the tunnel to allow for facile solvent access to the di-iron site.

The autoxidation $t_{1/2}$ of McHr is around ~50 min, which is much faster than that of hemerythrin from marine invertebrates, but significantly longer relative to that of DcrH-Hr. In the present study, we have mutated the L114 in McHr to F, Y and A. We find a 12- to 20-fold increase in the autoxidation $t_{1/2}$ of the L114F and L114Y McHr mutants relative to the WT McHr, rendering the autoxidation more akin to the behavior observed for the hemerythrins from marine animals. The observed longer time of autoxidation observed for the L114 McHr mutants suggests that this leucine plays the role of a water valve in the water tunnel of McHr. We surmise that Leu114 is serving as a hydrophobic barrier for passage of a water molecule from the water tunnel to the non-heme di-iron center. From the WT McHr high-resolution protein crystal structure, the diameter of the water tunnel is approximately 3.0–4.5 Å. This size of the water tunnel is wide enough to allow one water molecule to access the di-iron center of the McHr via passage across the Leu114 with the assistance of the hydrophobic repulsive force. There are no water molecules observed inside the water tunnel. The autoxidation rates that we have observed with the L114F and L114Y McHr mutants are consistent with this picture.

Evidently, hemerythrins can participate in dioxygen delivery, storage, or sensing in different organisms without distinct structural changes in the non-heme di-iron center in the various species. Indeed, the main difference between the bacterial Hrs and invertebrate Hrs is the water tunnel in the structural fold of the bacterial Hrs. The water tunnel is not found in invertebrate Hrs [15–17]. In the case of DcrH-Hr and McHr, where there is structural evidence for the water tunnel, the details of the water tunnel are also different (Fig. 9). In DcrH-Hr, the water tunnel passes from the left to right across the center of the protein surface from between α2 and α3 to between α1 and α4 [7,8]. The length of the putative tunnel between the metal center and the protein surface is also relatively short, which should lead to the observed fast rate of autoxidation. Unlike DcrH-Hr, the water tunnel in McHr penetrates just to the di-iron center without running through the two ends of the protein surface. The length of the tunnel is also relatively longer in McHr relative to DcrH-Hr.

In light of the above discussion, the oxy-from of invertebrate Hrs should be stable. Without a water tunnel, they would not be prone to the autoxidation reaction. Thus, a water tunnel is not required for a

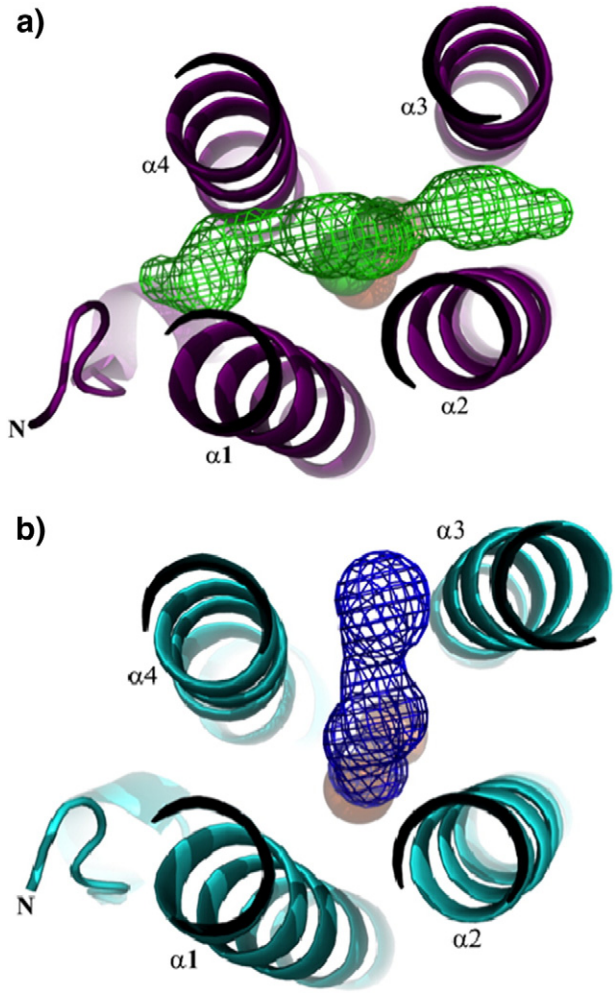

Fig. 9. Comparison of the putative water tunnel between DcrH-Hr and McHr. (a) Met-DcrH-Hr from *D. vulgaris* (PDB: 3AGT; purple), water tunnel is highlighted in green mesh. (b) Met-McHr from *M. capsulatus* (Bath) (light blue), water tunnel is shown in deep blue mesh.

hemerythrin that is functioning merely as storage for dioxygen. All hemerythrins shared the same highly conserved non-heme di-iron center for dioxygen binding. Due to its small size and nonpolar properties, a dioxygen molecule is able to gain access to the non-heme di-iron core of the protein by taking advantage of the micropores in the protein structure. The on–off rates of dioxygen binding to the non-heme di-iron center are rapid regardless of species, and whether or not there is a water tunnel in the hemerythrin. For example, in the case of DcrH-Hr, the k_{on} is $5.3 \times 10^8\ M^{-1}\ s^{-1}$ and k_{off} is $\sim 2 \times 10^3\ s^{-1}$ [30], orders of magnitude faster than the autoxidation rate constant even for this hemerythrin.

Finally, we address the issue of why autoxidation might be built into the design of the McHr. McHr is expressed in the cells of *M. capsulatus* (Bath) when this methanotroph is cultured and grown under high copper to biomass conditions to over-produce the pMMO [12]. At sufficiently high levels of pMMO in the intracytoplasmic membranes of the cell, the turnover of the pMMO becomes limited by the O_2 at the membrane interface, and McHr acts as a carrier to transport O_2 from the cytosol to the pMMO for the turnover of the enzyme [14]. Upon association with the pMMO, the O_2 would be rapidly released and transferred from the oxy-McHr to the pMMO. However, we surmise that when the O_2 is not consumed by the pMMO for methane oxidation for a prolonged period, for example, when there is no hydrocarbon substrate available to the pMMO, a mechanism is built to abort the oxy-McHr by autoxidation. Once converted to the met-form, the McHr can be dissociated from the pMMO and released from the membrane interface to the cytosol for re-reduction and eventual re-oxidation for another cycle of dioxygen transport and delivery. The autoxidation rate of McHr ($t_{1/2} \sim 50$ min) is consistent with this function of the hemerythrin.

Thus, by protein design, nature has evolved various hemerythrins for various functions, demonstrating once again that biochemical unity underlies biological diversity.

Abbreviations

McHr	bacteriohemerythrin in *Methylococcus capsulatus* (Bath)
pMMO	particulate methane monooxygenase
M. capsulatus (Bath)	*Methylococcus capsulatus* (Bath)
LB medium	Luria–Bertani medium
TEV protease	tobacco etch virus protease
FPLC	fast protein liquid chromatography
LMCT	ligand-to-metal charge transfer

Acknowledgments

This work was supported in part by grants MOST 99-2119-M-153-001 (to K.H.-C.C.) 101-2628-B-213-001-MY4, 102-2627-M-213-001-MY3 (to C.-J.C.), 101-2113-M-001-013 (to S.I.C.) and 101-2113-M-001-007-MY3 (to S.S.-F.Y.) from the Ministry of Science and Technology, Taiwan; and NPTU-AD-101-02 (to K.H.-C.C.) from the National Pingtung University (NPTU), Taiwan; and NSRRC 1023RSB02, 1023RSB14, 1033RSB02, and 1033RSB14 (to C.-J.C.) from the National Synchrotron Radiation Research Center (NSRRC), Taiwan. Academia Sinica provided support to S.I.C. and S.S.-F.Y. We are indebted to the supporting staffs on beamlines BL13B1, BL13C1 and BL15A1 at NSRRC, and Masato Yoshimura at the Taiwan-contracted beamline BL12B2 and beamline BL44XU at SPring-8 for the technical assistance. We are also grateful to Jyh-Fu Lee for assistance with the X-ray absorption measurements at NSRRC. Portions of this research were carried out at the NSRRC–NCKU Protein Crystallography Laboratory of the University Center for Bioscience and Biotechnology at National Cheng Kung University (NCKU).

Appendix A. Supplementary data

Supplementary data to this article can be found online at http://dx.doi.org/10.1016/j.jinorgbio.2015.04.001.

References

[1] I.M. Klotz, D.M. Kurtz Jr., Acc. Chem. Res. 17 (1984) 16–22.
[2] E.J. Wood, Essays Biochem. 16 (1980) 1–47.
[3] J.B. Dunn, A.W. Addison, R.E. Bruce, J. Sanders-Loehr, T.M. Loehr, Biochemistry 16 (1977) 1743–1749.
[4] P.M. Robitaille, D.M. Kurtz Jr., Biochemistry 27 (1988) 4458–4465.
[5] R.E. Stenkamp, Chem. Rev. 94 (1994) 715–726.
[6] N.B. Terwilliger, J. Exp. Biol. 201 (1998) 1085–1098.
[7] C.E. Isaza, R. Silaghi-Dumitrescu, R.B. Iyer, D.M. Kurtz Jr., M.K. Chan, Biochemistry 45 (2006) 9023–9031.
[8] A. Onoda, Y. Okamoto, H. Sugimoto, Y. Shiro, T. Hayashi, Inorg. Chem. 50 (2011) 4892–4899.
[9] Y. Okamoto, A. Onoda, H. Sugimoto, Y. Takano, S. Hirota, D.M. Kurtz Jr., Y. Shiro, T. Hayashi, Inorg. Chem. 52 (2013) 13014–13020.
[10] J. Xiong, D.M. Kurtz Jr., J. Ai, J. Sanders-Loehr, Biochemistry 39 (2000) 5117–5125.
[11] W.C. Kao, V.C. Wang, Y.C. Huang, S.S. Yu, T.C. Chang, S.I. Chan, J. Inorg. Biochem. 102 (2008) 1607–1614.
[12] W.C. Kao, Y.R. Chen, E.C. Yi, H. Lee, Q. Tian, K.M. Wu, S.F. Tsai, S.S. Yu, Y.J. Chen, R. Aebersold, S.I. Chan, J. Biol. Chem. 279 (2004) 51554–51560.
[13] O.A. Karlsen, L. Ramsevik, L.J. Bruseth, O. Larsen, A. Brenner, F.S. Berven, H.B. Jensen, J.R. Lillehaug, FEBS J. 272 (2005) 2428–2440.
[14] K.H. Chen, H.H. Wu, S.F. Ke, Y.T. Rao, C.M. Tu, Y.P. Chen, K.H. Kuei, Y.S. Chen, V.C. Wang, W.C. Kao, S.I. Chan, J. Inorg. Biochem. 111 (2012) 10–17.
[15] C.S. Farmer, D.M. Kurtz Jr., Z.J. Liu, B.C. Wang, J. Rose, J. Ai, J. Sanders-Loehr, J. Biol. Inorg. Chem. 6 (2001) 418–429.
[16] R.E. Stenkamp, L.C. Sieker, L.H. Jensen, J.E. McQueen Jr., Biochemistry 17 (1978) 2499–2504.
[17] W.A. Hendrickson, G.L. Klippenstein, K.B. Ward, Proc. Natl. Acad. Sci. U. S. A. 72 (1975) 2160–2164.

[18] S. Sheriff, W.A. Hendrickson, R.E. Stenkamp, L.C. Sieker, L.H. Jensen, Proc. Natl. Acad. Sci. U. S. A. 82 (1985) 1104–1107.
[19] J. Xiong, R.S. Phillips, D.M. Kurtz Jr., S. Jin, J. Ai, J. Sanders-Loehr, Biochemistry 39 (2000) 8526–8536.
[20] R. Chenna, H. Sugawara, T. Koike, R. Lopez, T.J. Gibson, D.G. Higgins, J.D. Thompson, Nucleic Acids Res. 31 (2003) 3497–3500.
[21] M.A. Larkin, G. Blackshields, N.P. Brown, R. Chenna, P.A. McGettigan, H. McWilliam, F. Valentin, I.M. Wallace, A. Wilm, R. Lopez, J.D. Thompson, T.J. Gibson, D.G. Higgins, Bioinformatics 23 (2007) 2947–2948.
[22] Z. Otwinowski, W. Minor, Methods Enzymol. 276 (1997) 307–326.
[23] M.D. Winn, C.C. Ballard, K.D. Cowtan, E.J. Dodson, P. Emsley, P.R. Evans, R.M. Keegan, E.B. Krissinel, A.G. Leslie, A. Mccoy, S.J. McNicholas, G.N. Murshudov, N.S. Pannu, E.A. Potterton, H.R. Powell, R.J. Read, A. Vagin, K.S. Wilson, Acta Crystallogr. D 67 (2011) 235–242.
[24] P. Emsley, K. Cowtan, Acta Crystallogr. D 60 (2004) 2126–2132.
[25] V.B. Chen, W.B. Arendall III, J.J. Headd, D.A. Keedy, R.M. Immormino, G.I. Kapral, L.W. Murray, J.S. Richardson, D.C. Richardson, Acta Crystallogr. D 66 (2009) 12–21.
[26] E. Chovancova, A. Pavelka, P. Benes, O. Strnad, J. Brezovsky, B. Kozlikova, A. Gora, V. Sustr, M. Klvana, P. Medek, L. Biedermannova, J. Sochor, J. Damborsky, PLoS Comput. Biol. 8 (2012) e1002708.
[27] C.S. Farmer, D.M. Kurtz Jr., R.S. Phillips, J. Ai, J. Sanders-Loehr, J. Biol. Chem. 275 (2000) 17043–17050.
[28] S. Jin, D.M. Kurtz Jr., Z.J. Liu, J. Rose, B.C. Wang, J. Am. Chem. Soc. 124 (2002) 9845–9855.
[29] S.V. Kryatov, E.V. Rybak-Akimova, S. Schindler, Chem. Rev. 105 (2005) 2175–2226.
[30] G.D. Armstrong, A.G. Sykes, Inorg. Chem. 25 (1986) 3135–3139.

Appendix A. Supplementary data:

Supplementary material 1:

The bacteriohemerythrin from *Methylococcus capsulatus* (Bath): Crystal structures reveal that Leu114 regulates a water tunnel

Kelvin H.-C. Chen[a,*,1], Phimonphan Chuankhayan[b,1], Hsin-Hui Wu[a,c], Chun-Jung Chen[b,d,e,*], Mitsuhiro Fukuda[f], Steve S.-F. Yu[g], Sunney I. Chan[g]

[a]*Department of Applied Chemistry, National Pingtung University, Pingtung, 90003, Taiwan*

[b]*Life Science Group, Scientific Research Division, National Synchrotron Radiation Research Center, 30076, Hsinchu, Taiwan*

[c]*Institute of Bioinformatics and Structural Biology and Structural Biology Program, National Tsing Hua University, Hsinchu, 30014, Taiwan*

[d]*Department of Biotechnology and Center for Bioscience and Biotechnology, National Cheng Kung University, Tainan, 701, Taiwan*

[e]*Department of Physics, National Tsing Hua University, Hsinchu, 30014, Taiwan*

[f]*Computer Chemistry Laboratory, Hyogo University of Teacher Education, 673-1494, Hyogo, Japan*

[g]*Institute of Chemistry, Academia Sinica, Taipei 11529, Taiwan*

[1] Co-first author

*Corresponding authors

Address: No.1 Lin-Sen Road, Pingtung City, 90003, Taiwan.
Tel: +886 8 7226141 ext.33254; Fax: +886 8 7230305.
E-mail: kelvin@mail.nptu.edu.tw (K. H.-C. Chen)

Address: No.101 Hsin-Ann Road, Hsinchu, 30076, Taiwan.
Tel: +886 3 5780281 ext.7330; Fax: +886 3 5783813.
E-mail: cjchen@nsrrc.org.tw (C.-J. Chen)

Figure Legends

Fig. A.1. SDS-PAGE analysis of the purified recombinant WT and McHr mutant proteins. Each lane contains 10 μg of the purified McHr proteins (WT, L114F, L114Y, and L114A) in 13.3% SDS-PAGE and is stained by coomassie blue staining to ensure protein purity. The molecular weight markers are indicated on the left column (kDa).

Fig. A.2. F_o-F_c maps showing the extra electron density (blue) in the water tunnel near the non-heme di-iron site in the L114A McHr mutant and fits of the extra electron density with a (**a**) sodium nitrate or (**b**) sodium acetate molecule. The structure refinement gives similar good density fitting with R_{work} and R_{free} values of 15.61 and 18.41% for Na nitrate (**a**) and 15.49 and 18.28% for Na acetate (**b**), respectively.

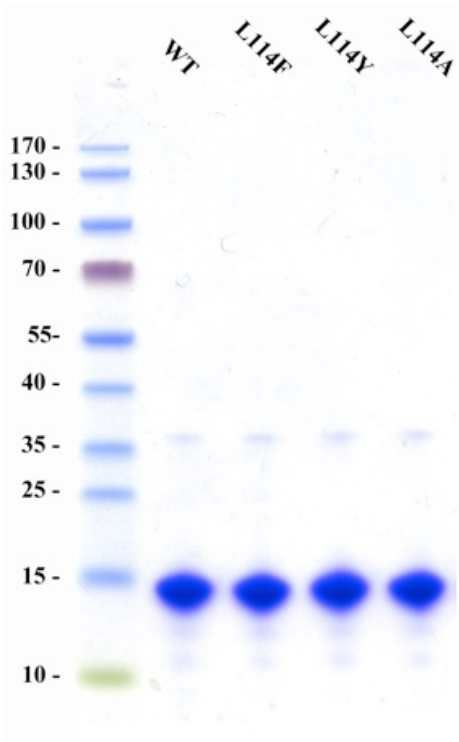

Fig. A.1. SDS-PAGE analysis of the purified recombinant WT and McHr mutant proteins. Each lane contains 10 μg of the purified McHr proteins (WT, L114F, L114Y, and L114A) in 13.3% SDS-PAGE and is stained by coomassie blue staining to ensure protein purity. The molecular weight markers are indicated on the left column (kDa).

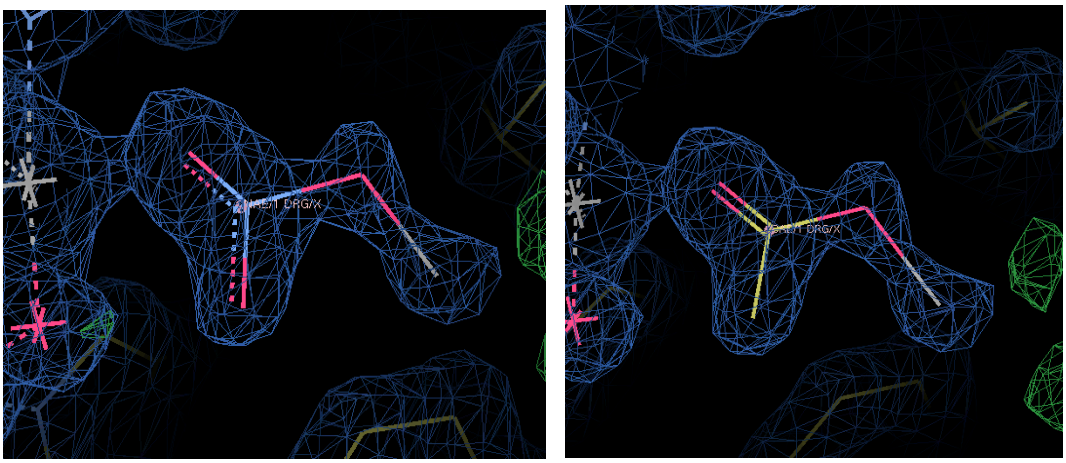

(a) **(b)**

Fig. A.2. F_o-F_c maps showing the extra electron density (blue) in the water tunnel near the non-heme di-iron site in the L114A McHr mutant and fits of the extra electron density with a (**a**) sodium nitrate or (**b**) sodium acetate molecule. The structure refinement gives similar good density fitting with R_{work} and R_{free} values of 15.61 and 18.41% for Na nitrate (**a**) and 15.49 and 18.28% for Na acetate (**b**), respectively.

Table. A.1. The primers used in the production of the L114A, L114F and L114Y mutants of McHr.

Primer	Sequence (5' - 3')
L114A F primer	5'-GGGTATGTGGTTGACCGCCCAGTCCCGTACGAAG-3'
L114A R primer	5'-CTTCGTACGGGACTGGGCGGTCAACCACATACCC-3'
L114F F primer	5'-GGGTATGTGGTTGACGAACCAGTCCCGTACGAAGC-3'
L114F R prime	5'-GCTTCGTACGGGACTGGTTCGTCAACCACATACCC-3'
L114I F primer	5'-GGGTATGTGGTTGACGATCCAGTCCCGTACGAAG-3'
L114I R primer	5'-CTTCGTACGGGACTGGATCGTCAACCACATACCC-3'
L114Y F primer	5'-GGGTATGTGGTTGACGTACCAGTCCCGTACGAAGC-3'
L114Y R primer	5'-GCTTCGTACGGGACTGGTACGTCAACCACATACCC-3'